Radiative Cooling Potential of a Water-Based Paint Formulation under Realistic Application Conditions

Radiative cooling potential of a water-based paint formulation under realistic application conditions

Giuseppe Emanuele Lio,[*,†,‡] Jérémy Werlé,[†,‡] Mariacarla Arduini,[¶] Diederik Sybolt Wiersma,[§,†,‡] Jochen Manara,[¶] and Lorenzo Pattelli[*,§,‡]

†*Department of Physics, University of Florence, 50019 Sesto Fiorentino, Florence*

‡*European Laboratory for Non Linear Spectroscopy, University of Florence, 50019 Sesto Fiorentino, Florence*

¶ *Center for Applied Energy Resarch (CAE), Magdalene-Schoch-Str. 3, 97074 Würzburg, Germany*

§*Natioanal Institute of Metrology (INRIM), Strada delle Caccie, Turin*

E-mail: lio@lens.unifi.it; lorenzo.pattelli@inrim.it

Abstract

Passive Radiative Cooling (PRC) technology holds promise to offset a significant fraction of our energy needs and carbon footprint associated to cooling. Among different approaches, paint-like systems present several advantages in terms of cost-effectiveness, scalability and application ease. However, most of the recent paint formulation capable of daytime PRC rely on the use of organic solvents which increase their cost, environmental impact, and safety hazards. Lightweight, water-based formulations are particularly desirable to suppress the emission of volatile organic compounds (VOCs) altogether and expand their applicability. We report on a simple paint mixture, with a solar reflectance of 90 % and a thermal emissivity of 95 %, comprising a

mixture of glass bubbles and PVDF-HFP used directly in its powder form. The paint is tested under conditions relevant for its application in the building sector, without sealing it from convection. Depending on the choice of the ambient temperature reference, a material with this degree of solar reflectance is found to exert either vanishing daytime cooling power, or up to $100\,\mathrm{W\,m^{-2}}$, highlighting the importance of rigorous testing and explaining the large performance variations found in the literature for PRC materials with similar spectral properties.

Keywords:

Passive Radiative Cooling; Water based paint; zero VOCs, glass bubbles; Thermal radiation; temperature drop; cooling power

INTRODUCTION

Global warming has led to higher temperatures and more frequent heatwaves, resulting in increased energy consumption for cooling, which accounts for a third of the total energy demand.[1,2] Cooling-related energy needs associated to air conditioning units are further expected to increase up by 750 % in 2050.[3] Traditional cooling technologies accelerate global warming due to their reliance on electricity, and the use of potent greenhouse gases as refrigerants, discharging additional excess heat into the environment, further aggravating the urban heat island effect and our collective cooling needs.[4–6]

The concept of daytime Passive Radiative Cooling (PRC) has recently emerged as a promising strategy to reduce cooling-related energy consumption in a fully passive way.[7,8] The PRC effects exploit the sky transparency window (STW) between 8 and 13 µm, at which infrared radiation can escape the Earth and dissipate into the heat sink of outer space. Combined with a high solar reflectance, the overall heat balance of a PRC coating can lead to its spontaneous cooling even during the day,[9] thus providing a net electricity-

free cooling power.[10–13] A schematic illustration related to the incoming solar radiation and the physical mechanism that provides a radiative exchange towards outer-space through the STW is reported in Figure 1 a.

Several strategies have been devised to simultaneously control the absorptivity in the solar spectrum and the emissivity at the mid-IR wavelengths of the STW. Nano- and micro-photonic structures and patterns have been used to enhance PRC effect,[14–16] even though their fabrication is still limited in terms of scalability. Paint-like systems represent a more versatile and cost-effective solution, containing different mixtures of nano and microparticles such as $CaCO_3$, $BaSO_4$, BN or SIO_2.[17–21] However, the extremely high particle densities typically associated with PRC paints requires the use of volatile organic solvents for their correct dispersion.[22] Additionally, materials as $BaSO_4$ can lead to paint coatings with very high weight per unit area compared to typical paint formulations, which may limit their applicability.

To overcome the limitation posed by the restrictions on the overall VOC content of paints, recent efforts are being directed towards the development of water-based coatings,[19,23–25] which should also be sufficiently lightweight and durable. A common approach to improve the scattering efficiency of a paint-like material while limiting its weight is to introduce a high porosity. A well-known example of a polymer material which exhibits selective emissivity and high UV resistance is the poly(vinylidene fluoride-co-hexafluoropropylene) (PVDF-HFP) co-polymer.[8] To increase its solar reflectance, PVDF-HFP is typically dissolved in acetone and a small quantity of water: the diverse evaporation rates of the solvent and non-solvent components result in a porous structure comprising pores at the nano and micro scale which are highly effective at scattering the broad spectral range. However, the substantial amount of solvent required to dissolve it and achieve this phase separation process leads to very high VOCs release in the environment and cost increase.

In this work, we describe a simple one-pot method to obtain a water-based acrylic paint formulation where durable and emissive PVDF-HFP is used directly in powder form. To

maintain a high porosity and a low weight, polydisperse glass bubbles[26–28] are also included, which contribute to a high scattering efficiency in the solar spectrum and increase emittance at near infrared wavelengths. Figure 1b depicts the functioning principle of the proposed paint formulation. Water-based formulations facilitate large-scale production and provide an avenue for energy conservation and more cooling load reduction in building cooling coatings.[29,30] The resulting VOCs-free paint formulation exhibits a solar reflectivity of 90 % and a STW emissivity of 95 % when applied to an aluminum substrate. Similar solar reflectance values are reported in the literature for PRC materials, with contrasting results. It can be expected that higher values are required to achieve a net cooling effect during daytime hours,[31–33] even though cooling measurements have also been reported for materials around 90 %. As we discuss in this work, these discrepancies may be attributed to two main factors: an over-estimation of the ambient temperature (which should be always measured outside of the sample measurement box[34]), and the measurement of spectral values not properly normalized against calibrated standards.[35]

The former point is particularly critical as it constitute the basis for claiming a sub-ambient cooling effect. As we show in the following, significant differences can be obtained depending on the quality of the Stevenson shield adopted, and its exposure to solar irradiance and ventilation.

MATERIALS AND METHODS

Paint manufacturing process

Our proposed paint formulation takes inspiration from previous examples using either $CaCO_3$, $BaSO_4$ or PVDF-HFP scatterers,[18,22,25] simplifying their formulation and avoiding the use of organic solvents. A water-based colorless acrylic base (density $1.05\,\mathrm{g\,cm^{-3}}$) was mixed manually with 33 w/v% of iM30k glass bubbles (density $0.62\,\mathrm{g\,cm^{-3}}$) from 3M and 26 w/v% of PVDF-HFP in powder form (density $1.71\,\mathrm{g\,cm^{-3}}$). This combination is able to provide a

lightweight mixture with two-fold benefits: high efficient scattering across the UV-VIS-NIR range given by the glass bubbles and the PVDF-HFP mixed in its powder form and, on the other hand, it improves the broad emissivity of the acrylic base and SiO_2 hollow spheres with the selective one in the STW given by PVDF-HFP copolymer.

Paint characterization

Optical and thermal characterization

The spectral directional-hemispherical reflectance R_{dh} and transmittance T_{dh} of the proposed samples has been measured at room temperature ($T = 300\,\mathrm{K}$) by an integrating sphere with a light source ranging from 0.25 µm to 35 µm. The spectral absorbance α_λ which, according to Kirchhoff's law, equals the spectral emittance ε_λ can be calculated from the spectral directional-hemispherical reflectance R_{dh} and transmittance T_{dh} as:

$$\alpha = 1 - R_{\mathrm{dh}} - T_{\mathrm{dh}} \tag{1}$$

In the wavelength range between 2.0 µm to 35 µm the samples are measured with a Bruker FTIR-spectrometer Vertex 70v. The wavelength range between 0.25 µm to 2.5 µm is covered by a Perkin Elmer Lambda 950 diffraction spectrometer. The thermal emittance $\varepsilon_{\mathrm{IR}}$ is then derived from the spectral emittance ε_λ, the latter gives the amount of thermal radiation that is emitted or absorbed by the surface perpendicular to its orientation. The normal thermal emittance $\varepsilon_{\mathrm{IR}}$ with respect to the temperature T can be calculated by integrating the spectral emittance ε_λ over all wavelengths with the Planck-function i_λ(T) as a weight function:

$$\varepsilon IR(T) = \frac{\int_{2\,\mu\mathrm{m}}^{35\,\mu\mathrm{m}} \varepsilon_\lambda(T) i_\lambda d\lambda}{\int_{2\,\mu\mathrm{m}}^{35\,\mu\mathrm{m}} i_\lambda d\lambda} \tag{2}$$

The Planck-function $i_\lambda(T)$ gives the intensity emitted by a black body at a certain temperature T. On the other hand, the solar reflectance R_{solar} is calculated by integrating the

spectral reflectance R_{dh} over all wavelengths with the solar radiation s_λ as weight function:

$$R_{\mathrm{solar}} = \frac{\int_{0.3\,\mu\mathrm{m}}^{2.5\,\mu\mathrm{m}} R_{\mathrm{dh}} s_\lambda d\lambda}{\int_{0.3\,\mu\mathrm{m}}^{2.5\,\mu\mathrm{m}} s_\lambda d\lambda} \tag{3}$$

Then the solar absorbance α_{solar} is derived from R_{solar} and T_{solar} as:

$$\alpha = 1 - R - T \tag{4}$$

The data reported in this work have been calibrated against a gold standard used as a reference, which was previously characterized by the German national metrology institute, the Physikalisch−Technische Bundesanstalt (PTB). Furthermore, the calculations about the visual, solar, UV reflectance and absorbance have been done in accordance with DIN EN 410 and ISO 9050 standards. The resulting normal thermal emittances $\varepsilon_{\mathrm{IR}}$ (thermal radiation that is emitted by the surface perpendicular to its orientation) and the hemispherical thermal emittance $\varepsilon_{h(T)}$ (thermal radiation that is emitted by the surface in the whole front hemisphere), was calculated in accordance with DIN EN 673 or DIN EN 12898 or ASTM E1585-93 from the spectral normal emittance ε_λ at ambient temperature ($T = 300\,\mathrm{K}$).

Morphological characterization

The morphological characterization has been done using a scanning electron microscope (SEM) Zeiss ULTRA plus with the use of "SmartSEM" as analysing software. Furthermore, the samples were not sputter coated (no metalization) to prevent sample surface alteration, while it has been used the method of charge compensation through added N_2 gas flow to allow discharge of the sample surface and prevent further accumulation of electrons. For the sample thickness analysis a Millitast 1085 has been involved.

Temperature and cooling power monitoring apparatus

The experimental setup used for the outdoor measurements consist of an home-built apparatus shown in Fig. 1 (c). The setup is composed by two main acquisition boards used for the temperature drop (Tdrop) and the cooling power (Pcool) density evaluation. The Tdrop board is equipped with NTC (Negative Temperature Coefficient) probes to measure the temperature of the samples, and DHT22 sensors to measure the relative ambient temperature T_{amb} and humidity. Additionally, a light sensor monitors the sunlight irradiance and a IR sensors to monitor the apparent sky temperature and the presence of clouds. On the other hand, the Pcool board is equipped with a Proportional-Integral-Derivative (PID) control which is fed with ambient temperature readings to drive a resistive heater. Aluminum sample holders are designed to host a temperature sensor internally, and placed on an expanded polystyrene base to ensure their thermal insulation from the surrounding. Finally, three independent estimates of ambient temperature are monitored using a professional PVC Stevenson shield (Davis 7714 – passive radiation shield) and ABS lightweight (cheaper) version placed under the same conditions, or shaded from direct sunlight. In Figure 1c is reported the setup equipped only with the ABS Stevenson shield, while in Figure 1d is reported the case with multiple solar screens installed including the aforementioned PVC one. This allows to obtain different apparent ΔT values depending on the ambient temperature reference. A negative difference signals that the sample is colder than the target ambient temperature reference. The measurement box is shielded with aluminum foil to avoid radiative heat ingress from the sun, and surrounded by PE walls to reduce direct wind. Two samples are tested simultaneously for reproducibility, which are kept in contact with external air without any additional convection shield.

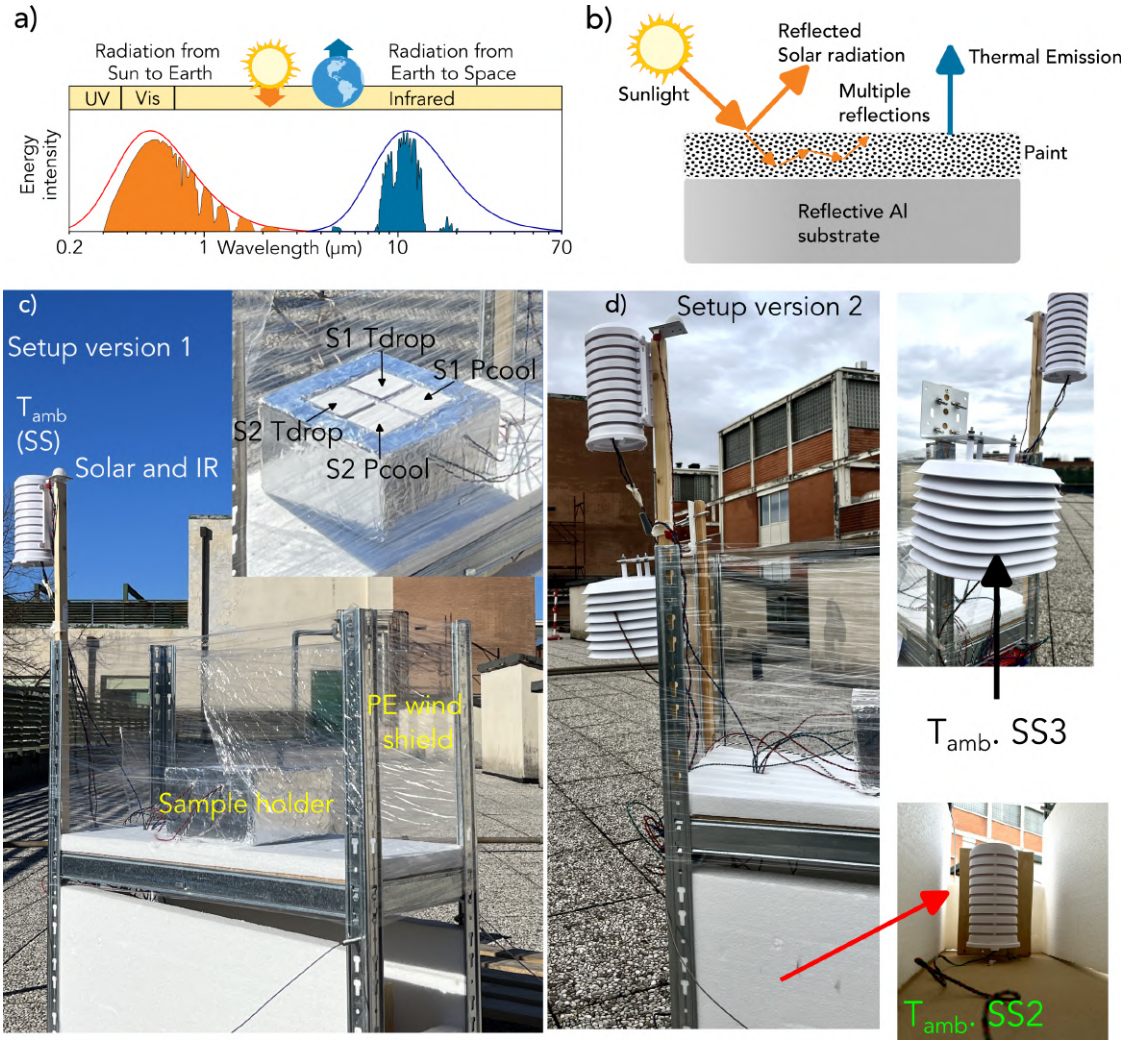

Figure 1: a) Schematics of the passive radiative cooling principle, showing the solar spectrum (ASTM G173, orange) and the sky transparency window (blue). b) Sketch of the paint sample comprising 3M glass bubbles (iM30k), and PVDF-HFP (Arkema Kynar Flex 2801) particles, deposited on an aluminum substrate. c-d) Photographs of the outdoor experimental setup equipped with a Stevenson screens of low (SS1 and SS2) and high (SS3) quality, placed in different positions.

RESULTS AND DISCUSSION

Optical Characterization

Our proposed paint formulation is mixed manually and applied onto a reflective aluminum substrate using a brush. Multiple coats are applied until no additional reflectivity increase is observed, this phenomenon is confirmed for the proposed paint after three coats (Figure 2). In particular, solar reflectance is shown to increase from 85.4 % for a single coat, 87.6 % for double coat, 89.9 % for three coats and finally 89.9 % for four coats. On the other hand, the normal thermal emittance is 95 % and the hemispherical thermal emittance is 89 % for all samples. Hence, the selected sample for the spontaneous radiative cooling tests is the aluminum substrate coated by three paint layers. The physical behavior can be summarized considering the acrylic paint dense of glass bubbles and PVDF-HFP as a scattering medium able to reflect the solar radiation that impinges on it, avoiding mainly the solar light absorption across λ=400 nm and λ=1500 nm and reducing it in the remaining solar spectrum. While, the proposed formulation is drastically improving the features in the long wave infrared range passing by zero, given by the pristine aluminum substrate, to a high emittance specially in the sky transparent window.

Morphological Characterization

A morphology analysis of the external surface and internal cross-section of the samples was performed via electron microscopy, showing the roughness of the sample surface introduced by the brush application, and the dense arrangement of the polydisperse glass bubbles, which roughly span a diameter range between 2 µm and 18 µm (Figure 3.) As a further characterization, the thickness of each sample with varying numbers of applied coats has been measured. These measurements were conducted at five different points on each surface to assess how the roughness resulting from brush application might influence the overall surface morphology. Table 1 presents the thickness data for the substrate used and the

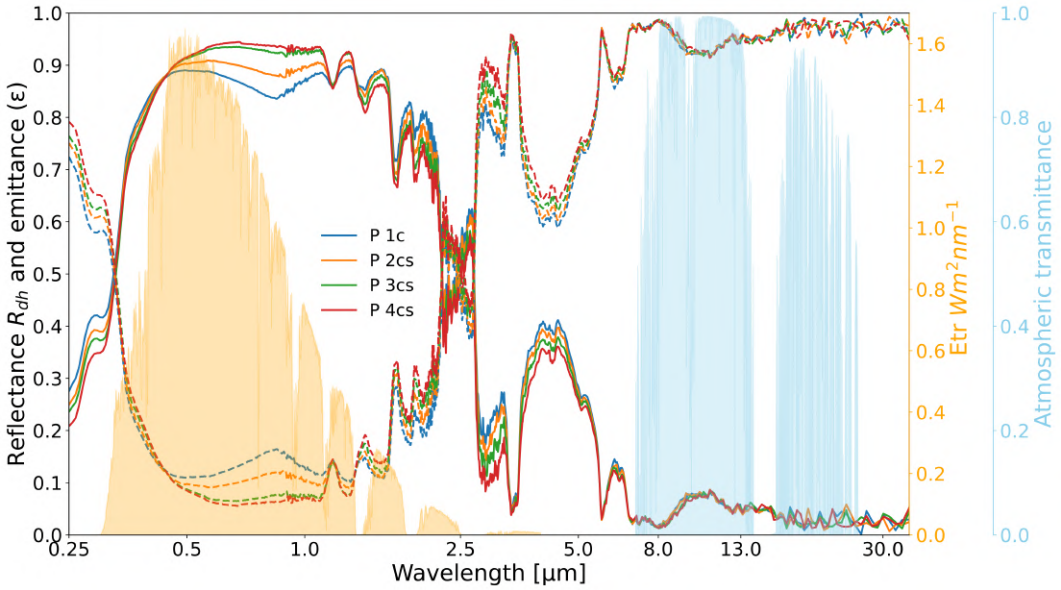

Figure 2: Experimental measures of reflectance R_{dh} (solid lines) and emittance ε (dashed lines) for the proposed paint using different coats (from 1 coat, 1c, up to four, 4 cs). The plots have been overlapped to the ASTM G173 (solar spectrum in orange) and the atmospheric transmittance (blue area).

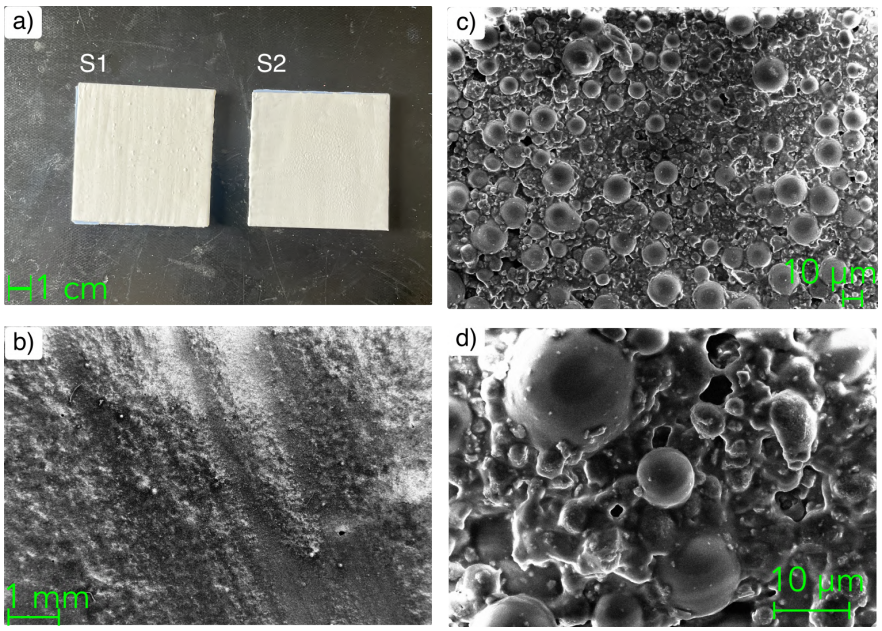

Figure 3: a) photograph of the sample S1 and S2. SEM images about b) a large area of the sample surface highlighting the morphology produced by the use of a brush to apply the paint. c-d) details about the arrangements of the glass bubbles in the sample.

samples with different numbers of coating layers. Based on the measurements, the average roughness value for each sample is approximately 0.11 mm, which translates to around 9 % of the total thickness.

Table 1: Comparative table about sample thickness varying the number of coats.M# stands for measurements, <M>is the average of the measurements, and sub. stands for the substrate thickness.

Sample:	M1 (mm)	M2 (mm)	M3 (mm)	M4 (mm)	M5 (mm)	<M>- sub. (mm)	Err (mm)
Substrate	0.52	0.52	0.52	0.53	0.52	0.523-0.523	
1 coat	0.82	0.84	0.86	0.88	0.84	0.33	0.02
2 coats	1.02	1.08	1.04	0.92	1.00	0.49	0.04
3 coats	1.39	1.51	1.48	1.50	1.44	0.94	0.04
4 coats	1.76	1.79	1.71	1.71	1.76	1.23	0.03

Surface self-cleaning

A paint including glass bubbles and PVDF−HFP in its formulation offers an advantage in terms of augmenting surface strength against paint transfer and soiling, as evidenced in Figure 4. In order to assess the paint mechanical resilience (abrasion and paint transfer) involves subjecting the surface to testing with a soaked black rough cloth. Notably, the absence of paint transfer, under rubbing, is indicative of the paint durability. This test is reported in the SI see Movie1, and in the two extrapolated frames reported in Figure 4 a.1 and a.2. Further tests on the proposed paint have been conducted, in the first one we soiled with dust the surface and the cleaned it by water demonstrating the paint facile cleaning, as reported in SI see Movie2, and in the frames shown in Figure 4 b.1 and b.2. Subsequently, the surface was soiled with three distinct dyes known for their strong coloration and substrate-bonding capabilities: methylene blue, brilliant yellow, and dimethyl sulfide. The subsequent water washes restored the surface pristine condition, underscoring also the self-cleaning against stains. This test is shown in SI Movie3, and depicted through two frames in Figure 4 c.1 and c.2

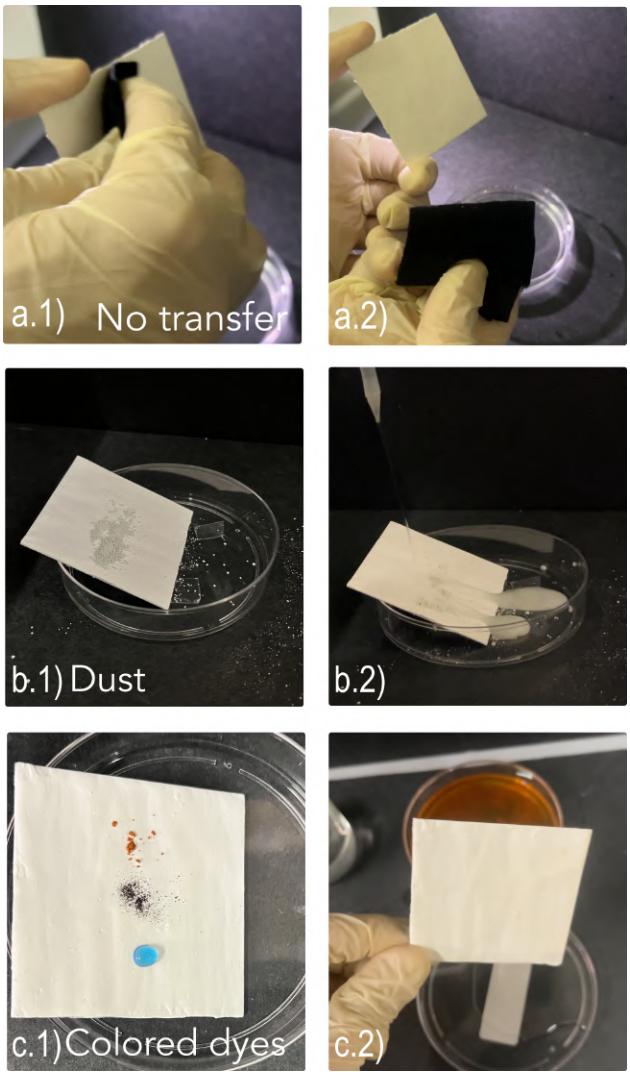

Figure 4: a.1 a.2) pictures of the no transfer test using a soaked rough black cloth. b.1 b.2) pictures of the paint soiled with dust and cleaned with water. c.1 c.2) pictures of the paint solied using colored dyes and then cleaned using water.

Experimental measurements of the cooling performance

The cooling performance of the proposed paint formulation was performed in January, February and April 2024 under different conditions, using Stevenson screens of different qualities during the first and second round of measurements, while the third one has been used to confirm the previous results and the material stability. During the January session, a standard setup implementation was realized using a lightweight solar screen (identifiable as "low quality" or "cheap") made of ABS plastic to measure ambient temperature outside the sample box. To verify the reliability of the temperature reading obtained inside this screen, a new measurement session was planned in February, including a second identical ABS screen placed in the shades and a "professional" more heavily shielded PVC screen placed under direct sunlight.".

Figure 5a shows the ambient temperature and the sample temperature during the first two days of measurements in January, which were characterized by a moderate humidity, a solar irradiance of maximum $350\,\mathrm{W\,m^{-2}}$, and a clear sky (IR temperature between $-30°$ and 0°C) as reported in Figure 5b. As can be seen from Figure 5c, the temperature drop characterization measuring the ambient temperature using cheap Stevenson shield under direct sunlight suggests that the painted substrates are cooling to sub-ambient temperatures between $-2\,°\mathrm{C}$ and $-9\,°\mathrm{C}$ during a 24 h cycle, with corresponding cooling powers estimated between 10 and $100\,\mathrm{W\,m^{-2}}$ (Figure 5d). In all the experimental measurements the shaded area represents the temperature variation considering the difference between S1 and S2. Significantly different results are obtained on the following month for the temperature drop and the cooling power, as a consequence of using an ambient temperature reference measured with a professional Stevenson shield, and despite the otherwise similar ambient conditions. In fact, as can be seen from Figure 6a, the temperature measured inside the high quality Stevenson shield (SS3) was significantly lower than that obtained in the other two, even compared to the shaded one. In Figure 6b are reported the relative humidities ranging between 35 % and 75 %, the solar irradiance with a maximum of $430\,\mathrm{W\,m^{-2}}$, and the clear sky (low

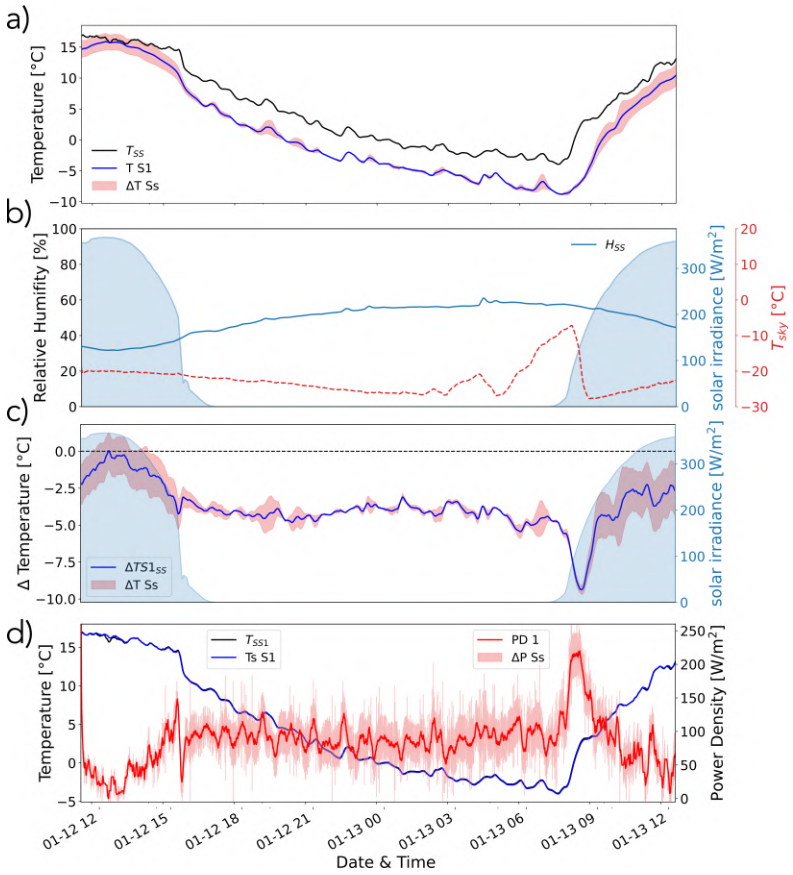

Figure 5: a) Measurements of T_{amb} within the low-quality Stevenson shield under sunlight (SS), along with sample temperatures TS1 black, and blue solid lines, respectively. The shaded area represents the uncertainty calculated as the difference between the temperatures measured for the identical sample pair S1 and S2. b) Relative humidity measurements obtained within the SS, solar irradiation (depicted as the blue area) and infrared (IR) sky temperature (red dashed line). c) Comparison of net temperature drop measures (ΔT) for samples S1 (red solid line) and S2 (blue solid line) in relation to T_{amb} recorded inside SS. The irradiance curve is represented on the right Y-axis. d) Sample temperatures of the warmed-up samples using T_{amb} as the set point. f) Power density plot showcasing samples S1 (red solid line), while shaded area is the difference between the power densities measured for the identical two samples.

sky IR temperature $-15°$ and 0°C) for these two experiment days. The differences between the readings obtained with the three different Stevenson shields are further summarized in Figure 6. The plot shows a comparison between: Tamb inside SS3 and Tamb inside SS1 (orange solid line), and Tamb inside SS3 and Tamb inside SS2 (green solid line). This analysis shows that even a measurement performed following the best practice of measuring ambient temperature in a Stevenson shield outside of the sample measurement box[34] can lead to a significant overestimation of the temperature drop provided by a PRC sample if a low quality solar screen is used, since the associated ambient temperature can be up to 5 °C hotter than the true ambient temperature. Surprisingly, the situation is only slightly improved by measuring ambient temperature in a shaded region, since also in this case the temperature is over-estimated during daytime hours by roughly 1.5 °C. During the night, all temperatures eventually converge to the same values, which is why nighttime data should always be included in experimental measurement campaigns of the cooling performance of PRC materials. Moreover, the results in terms of T_{amb} and the relative humidity measured using inside SS3, and the irradiance are in good agreement with the meteorological weather station hosted close to our research center, all the data are available on the following open-access LAMMA website.

When compared to this additional ambient temperature (SS3) reference, it can be seen that the cooling power provided by the samples is not sufficient to reach sub-ambient temperatures (Figures 7a-c). Figure 7a shows the ambient temperature measured in SS3 and the sample temperature during the measurements performed in February. As can be seen from Figure 7b, the temperature drop referred to the reading of the professional Stevenson shield (SS3) under direct sunlight, reveals that the paints cannot reach sub-ambient temperatures during the daytime, while a ΔT comprised between -6 °C and 0 °C is observed during the nighttime, see the blue dashed lines in the plot. On the other hand, when using the SS1 reading as the reference ambient temperature, sub-ambient cooling between -1 °C and -6 °C is observed during a 24 h cycle (solid blue line), in agreement with the previous measurement

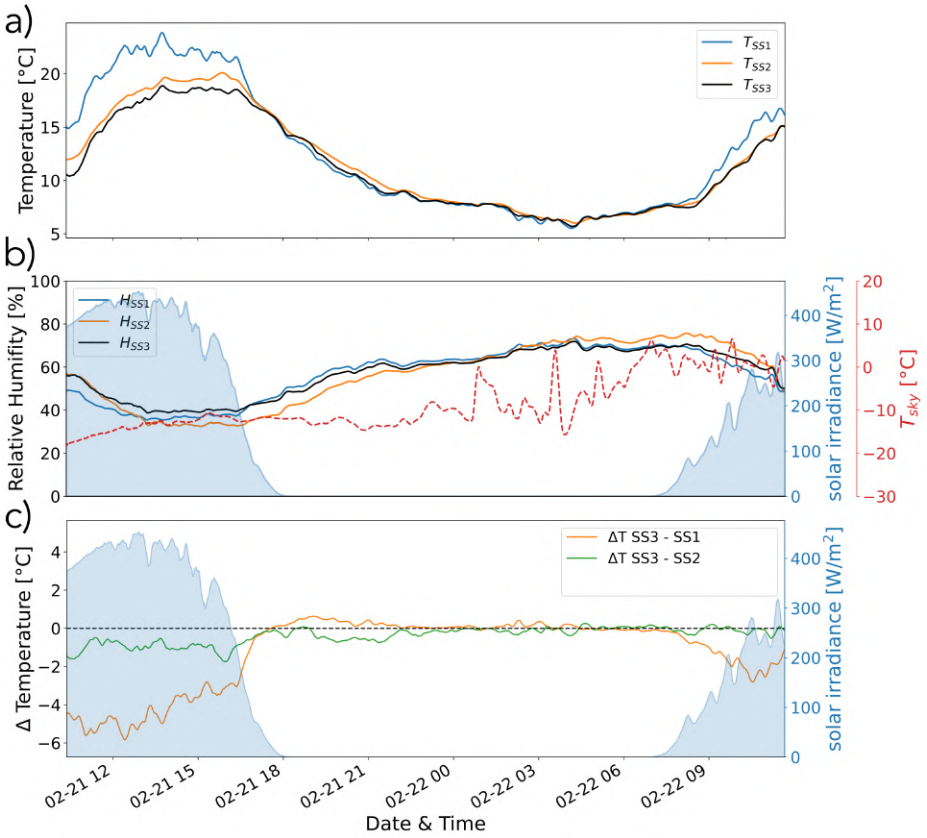

Figure 6: a) Measurements of ambient temperature (T_{amb}) inside different Stevenson shields under sunlight: SS1 (light blue solid line), SS2 placed in the shadow (orange solid line), and SS3 professional shield (black solid line). b) Relative humidity measurements obtained within the Stevenson shields, solar irradiation (depicted as the blue area) and infrared (IR) sky temperature (red dashed line). c) Ambient temperature differences (ΔT_{amb}) between: T_{amb} inside SS3 and T_{amb} inside SS1 (orange solid line), and T_{amb} inside SS3 and T_{amb} inside SS2 (green solid line).

session in January. Figure 7c reports the corresponding cooling powers considering the ambient temperature measured in SS3 as the PID setting point. The cooling power estimated is ranging between 0 and 100 $\mathrm{W\,m^{-2}}$. As discussed and expected during the daytime there is no cooling power for the proposed sample. In all the experimental measurements the shaded area represents the temperature uncertainty considering the difference between S1 and S2. In April, 4 months after samples realization, a new test was conducted using again all three

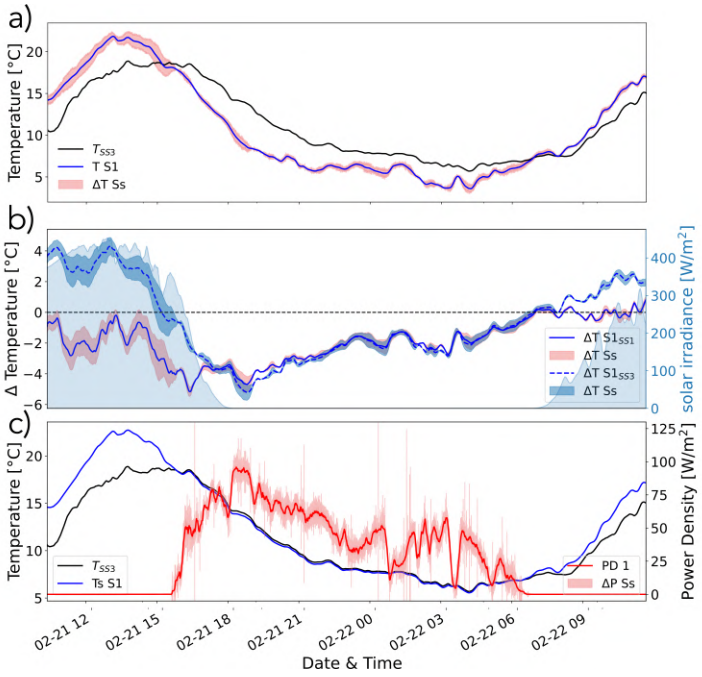

Figure 7: a) Ambient temperatures T_{SS3}, along with sample temperatures T S1 black, and blue solid lines, respectively. The shaded area represents the uncertainty calculated as the difference between the temperatures measured for the identical sample pair S1 and S2. b) Comparison of net temperature drop measures (ΔT) for samples S1 (blue dashed line with its uncertainty) against T_{amb} measured in SS3. The irradiance curve is represented on the right y-axis. c) Temperature of the warmed-up sample (blue solid line) using T_{amb} inside SS3 as the set point (black solid line). Power density plot showcasing samples S1 (red solid line), while shaded area is the difference between the power densities measured for the identical two samples.

Stevenson shields. Figure 8a shows the ambient temperature measured in SS3 and the sample temperature during the measurements performed during this third session. In Figure 8b, the relative humidity ranging between 35 % and 80 %, the solar irradiance with a maximum of 600 $\mathrm{W\,m^{-2}}$, and the clear sky (low sky IR temperature $-15°$ and 0°C) for these experi-

ment days are reported. As can be seen from Figure 8c temperature drop characterization, performed by measuring the ambient temperature using the professional Stevenson shield (SS3) under direct sunlight, highlights how the paints are not able to cooling down 5 °C and 0 °C during the daytime while they are cooling during the nighttime and the ΔT comprised btween -5 °C and 0 °C, see the blue dashed lines in the plot. Figure 8d reports the corresponding cooling powers (red line and shaded area) considering the ambient temperature measured in SS3 as the PID setting point (black solid line). The cooling power estimated is ranging between 0 and 120 $\mathrm{W\,m^{-2}}$. As discussed and expected during the daytime there is no cooling power for the proposed sample. In all the experimental measurements, as previously done, the shaded area represents the temperature variation considering the difference between S1 and S2. The three different measurement sessions carried out over four months allow us to highlight the stability of the material. It is important not to overlook that there were variations in weather conditions, such as ambient temperature, relative humidity and IR sky temperature, on the other hand, due to the fact that this material is mainly a nighttime cooler and all ambient temperature measurements (performed inside the low and professional quality Stevenson shields) slowly converge to the same value during the night hours, the material recovers the previously determined temperature drop and cooling power values, as expected, in all experimental session.

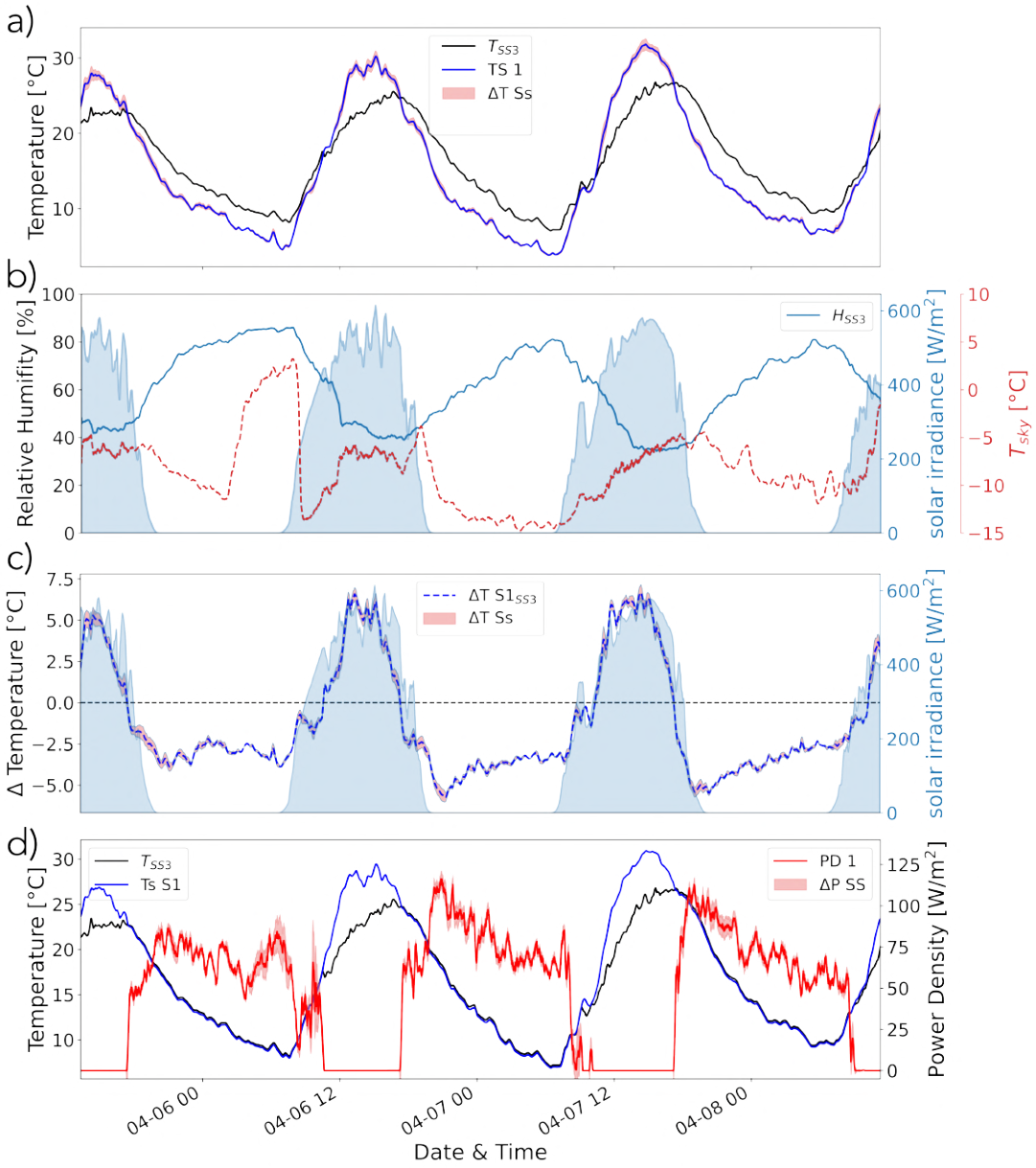

Figure 8: a) Ambient temperatures T_{SS1} and T_{SS3}, along with sample temperatures T S1 light blue, black, and blue solid lines, respectively. The shaded area represents the uncertainty calculated as the difference between the temperatures measured for the identical sample pair S1 and S2. b) Relative humidity measurements obtained within the Stevenson shields, solar irradiation (depicted as the blue area) and infrared (IR) sky temperature (red dashed line). c) Net temperature drop measures (ΔT) for samples S1 (blue solid line with its uncertainty) against T_{amb} measured in SS1. The same comparison with T_{amb} measured inside SS3 is reported using dashed line. The irradiance curve is represented on the right y-axis. d) Temperature of the warmed-up sample (blue solid line) using T_{amb} inside SS3 as the set point (black solid line). Power density plot showcasing samples S1 (red solid line), while shaded area is the difference between the power densities measured for the identical two samples.

CONCLUSIONS

In this work, we reported on the fabrication of a simple paint-like formulation made of an acrylic base mixed with glass bubbles and PVDF-HFP powder. Thanks to its water-based formulation, the resulting paint has zero VOCs emissions. With an application of 3 coats on an aluminum substrate, the paint reaches a solar reflectance of about 90 %, which is shown to be below the threshold needed to provide a net daytime cooling when the paint is tested without convective shielding, and compared to the true external ambient temperature. These results highlight the importance of testing candidate PRC materials under realistic conditions, avoiding the potential over-heating effect of sealed measurement test boxes (especially in the case of cooling power measurements, where the box contains a heating element), normalizing their spectral response to calibrated standards, and using high-end solar shielding to minimize systematic biases in the estimation of the ambient temperature set point.

Acknowledgement

The authors thank Roberto Concas for technical support during the preparation of the measurement apparatus. Part of this work is supported by the European project PaRaMetriC, code 21GRD03. The project 21GRD03 PaRaMetriC received funding from the European Partnership on Metrology, co-financed by the European Union's Horizon Europe Research and Innovation Programme and from the Participating States. G.E.L. acknowledges support from the "FSE-REACT EU" program financed by National Social Fund–National Operative Research Program and Innovation 2014-2020 (D.M. 1062/2021), personal Grant number 10-G-15049-2. J.W. acknowledges co-funding by the European Union - PON Research and Innovation 2014-2020 in accordance with Article 24, paragraph 3a), of Law No. 240 of December 30, 2010, as amended, and Ministerial Decree No. 1061 of August 10, 2021.

References

(1) Family, R.; Mengüç, M. P. Materials for radiative cooling: a review. *Procedia environmental sciences* **2017**, *38*, 752–759.

(2) Khosla, R.; Miranda, N. D.; Trotter, P. A.; Mazzone, A.; Renaldi, R.; McElroy, C.; Cohen, F.; Jani, A.; Perera-Salazar, R.; McCulloch, M. Cooling for sustainable development. *Nature Sustainability* **2021**, *4*, 201–208.

(3) Santamouris, M. Cooling the buildings–past, present and future. *Energy and Buildings* **2016**, *128*, 617–638.

(4) Birol, F. The future of cooling: opportunities for energy-efficient air conditioning. *International Energy Agency* **2018**, *526*, 1.

(5) Brown, J. S.; Domanski, P. A. Review of alternative cooling technologies. *Applied Thermal Engineering* **2014**, *64*, 252–262.

(6) Cook, B. I.; Smerdon, J. E.; Seager, R.; Coats, S. Global warming and 21 st century drying. *Climate dynamics* **2014**, *43*, 2607–2627.

(7) Raman, A. P.; Anoma, M. A.; Zhu, L.; Rephaeli, E.; Fan, S. Passive radiative cooling below ambient air temperature under direct sunlight. *Nature* **2014**, *515*, 540–544.

(8) Mandal, J.; Fu, Y.; Overvig, A. C.; Jia, M.; Sun, K.; Shi, N. N.; Zhou, H.; Xiao, X.; Yu, N.; Yang, Y. Hierarchically porous polymer coatings for highly efficient passive daytime radiative cooling. *Science* **2018**, *362*, 315–319.

(9) Hossain, M. M.; Gu, M. Radiative cooling: principles, progress, and potentials. *Advanced Science* **2016**, *3*, 1500360.

(10) Miller, J. L. Passive cooling doesn't cost the planet. *Physics today* **2017**, *70*, 16–18.

(11) Chu, S.; Cui, Y.; Liu, N. The path towards sustainable energy. *Nature materials* **2017**, *16*, 16–22.

(12) Ding, Z.; Li, H.; Li, X.; Fan, X.; Jaramillo-Fernandez, J.; Pattelli, L.; Zhao, J.; Niu, S.; Li, Y.; Xu, H. Designer SiO2 Metasurfaces for Efficient Passive Radiative Cooling. *Advanced Materials Interfaces* **2023**, 2300603.

(13) Li, X.; Ding, Z.; Lio, G. E.; Zhao, J.; Xu, H.; Pattelli, L.; Pan, L.; Li, Y. Strain-adjustable reflectivity of polyurethane nanofiber membrane for thermal management applications. *Chemical Engineering Journal* **2023**, *461*, 142095.

(14) Wang, T.; Wu, Y.; Shi, L.; Hu, X.; Chen, M.; Wu, L. A structural polymer for highly efficient all-day passive radiative cooling. *Nature communications* **2021**, *12*, 365.

(15) Liu, S.; Sui, C.; Harbinson, M.; Pudlo, M.; Perera, H.; Zhang, Z.; Liu, R.; Ku, Z.; Islam, M. D.; Liu, Y.; others A Scalable Microstructure Photonic Coating Fabricated by Roll-to-Roll "Defects" for Daytime Subambient Passive Radiative Cooling. *Nano Letters* **2023**, *23*, 7767–7774.

(16) Ding, Z.; Li, X.; Zhang, H.; Yan, D.; Werlé, J.; Song, Y.; Pattelli, L.; Zhao, J.; Xu, H.; Li, Y. Robust radiative cooling via surface phonon coupling-enhanced emissivity from SiO2 micropillar arrays. *International Journal of Heat and Mass Transfer* **2024**, *220*, 125004.

(17) Atiganyanun, S.; Kumnorkaew, P. Effects of pigment volume concentration on radiative cooling properties of acrylic-based paints with calcium carbonate and hollow silicon dioxide microparticles. *International Journal of Sustainable Energy* **2023**, *42*, 612–626.

(18) Li, X.; Peoples, J.; Huang, Z.; Zhao, Z.; Qiu, J.; Ruan, X. Full daytime sub-ambient radiative cooling in commercial-like paints with high figure of merit. *Cell Reports Physical Science* **2020**, *1*, 1–12.

(19) Huang, W.; Chen, Y.; Luo, Y.; Mandal, J.; Li, W.; Chen, M.; Tsai, C.-C.; Shan, Z.; Yu, N.; Yang, Y. Scalable aqueous processing-based passive daytime radiative cooling coatings. *Advanced Functional Materials* **2021**, *31*, 2010334.

(20) Du, T.; Niu, J.; Wang, L.; Bai, J.; Wang, S.; Li, S.; Fan, Y. Daytime Radiative Cooling Coating Based on the Y2O3/TiO2 Microparticle-Embedded PDMS Polymer on Energy-Saving Buildings. *ACS Applied Materials & Interfaces* **2022**, *14*, 51351–51360.

(21) Felicelli, A.; Katsamba, I.; Barrios, F.; Zhang, Y.; Guo, Z.; Peoples, J.; Chiu, G.; Ruan, X. Thin layer lightweight and ultrawhite hexagonal boron nitride nanoporous paints for daytime radiative cooling. *Cell Reports Physical Science* **2022**, *3*, 1–17.

(22) Li, X.; Peoples, J.; Yao, P.; Ruan, X. Ultrawhite BaSO4 paints and films for remarkable daytime subambient radiative cooling. *ACS Applied Materials & Interfaces* **2021**, *13*, 21733–21739.

(23) Xue, X.; Qiu, M.; Li, Y.; Zhang, Q.; Li, S.; Yang, Z.; Feng, C.; Zhang, W.; Dai, J.-G.; Lei, D.; others Creating an eco-friendly building coating with smart subambient radiative cooling. *Advanced Materials* **2020**, *32*, 1906751.

(24) Zhao, Y.; Pang, D.; Chen, M.; Chen, Z.; Yan, H. Scalable aqueous processing-based radiative cooling coatings for heat dissipation applications. *Applied Materials Today* **2022**, *26*, 101298.

(25) Gong, Q.; Lu, L.; Chen, J.; Lau, W. Y.; Cheung, K. H. A novel aqueous scalable eco-friendly paint for passive daytime radiative cooling in sub-tropical climates. *Solar Energy* **2023**, *255*, 236–242.

(26) Nie, X.; Yoo, Y.; Hewakuruppu, H.; Sullivan, J.; Krishna, A.; Lee, J. Cool white polymer coatings based on glass bubbles for buildings. *Scientific reports* **2020**, *10*, 6661.

(27) Yu, X.; Yao, F.; Huang, W.; Xu, D.; Chen, C. Enhanced radiative cooling paint with broken glass bubbles. *Renewable Energy* **2022**, *194*, 129–136.

(28) Jiang, K.; Zhang, K.; Shi, Z.; Li, H.; Wu, B.; Mahian, O.; Zhu, Y. Experimental and numerical study on the potential of a new radiative cooling paint boosted by SiO2 microparticles for energy saving. *Energy* **2023**, *283*, 128473.

(29) Mandal, J.; Yang, Y.; Yu, N.; Raman, A. P. Paints as a scalable and effective radiative cooling technology for buildings. *Joule* **2020**, *4*, 1350–1356.

(30) Lin, K.; Chao, L.; Ho, T. C.; Lin, C.; Chen, S.; Du, Y.; Huang, B.; Tso, C. Y. A flexible and scalable solution for daytime passive radiative cooling using polymer sheets. *Energy and Buildings* **2021**, *252*, 111400.

(31) Li, X.; Pattelli, L.; Ding, Z.; Chen, M.; Zhao, T.; Li, Y.; Xu, H.; Pan, L.; Zhao, J. A Novel BST@ TPU Membrane with Superior UV Durability for Highly Efficient Daytime Radiative Cooling. *Advanced Functional Materials* **2024**, 2315315.

(32) Sun, J.; Wang, J.; Guo, T.; Bao, H.; Bai, S. Daytime passive radiative cooling materials based on disordered media: A review. *Solar Energy Materials and Solar Cells* **2022**, *236*, 111492.

(33) Chen, M.; Pang, D.; Chen, X.; Yan, H.; Yang, Y. Passive daytime radiative cooling: Fundamentals, material designs, and applications. *EcoMat* **2022**, *4*, e12153.

(34) Zhou, L.; Yin, X.; Gan, Q. Best practices for radiative cooling. *Nature Sustainability* **2023**, *6*, 1030–1032.

(35) Bu, K.; Huang, X.; Li, X.; Bao, H. Consistent Assessment of the Cooling Performance of Radiative Cooling Materials. *Advanced Functional Materials* **2023**, *33*, 2307191.

TOC Graphic

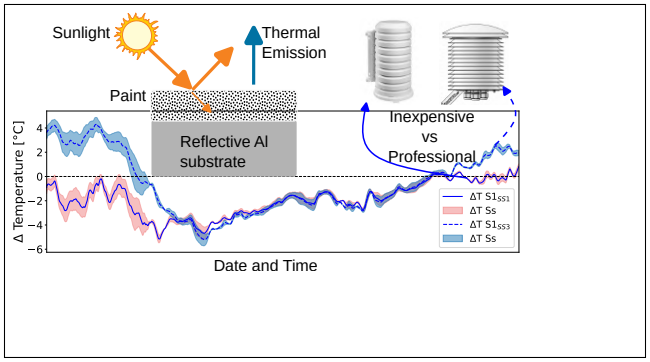
Sunlight
Thermal
Emission
Paint
Reflective Al
substrate
Inexpensive
vs
Professional
Δ Temperature [°C]
Date and Time
ΔT S1SS1
ΔT Ss
ΔT S1SS3
ΔT Ss